

Experimental Investigation of Initial Onset of Sand Deposition in the Turbine Section of Gas
Turbines

Hardik Dipan Patel

Thesis submitted to the faculty of the Virginia Polytechnic Institute and State University in
partial fulfillment of the requirements for the degree of

Master of Science
In
Mechanical Engineering

Wing F. Ng, Chair
Srinath V. Ekkad, Co-chair
Gary R. Pickrell

June 5, 2015
Blacksburg, VA

Keywords: Sand Ingestion, Particle Concentration, Deposition, Particle Impact, High
Temperature

Copyright 2015

Experimental Investigation of Initial Onset of Sand Deposition in the Turbine Section of Gas Turbines

Hardik Dipan Patel

ABSTRACT

Particle ingestion and deposition is an issue of concern for gas turbine engines operating in harsh environments. The ingested particles accelerate the deterioration of engine components and thus reduce its service life. This effect is observed to a greater extent in aircrafts/helicopters operating in particle laden environment. Understanding the effects of particle ingestion at engine representative condition leads to improved designs for turbomachinery. Experiments have been in an Aerothermal Rig facility at Virginia Tech to study particle deposition at engine representative temperatures. The Aerothermal Rig was upgraded to achieve air temperatures of up to 1100°C at the test section. The experiments are performed using Arizona Road Dust (ARD) of 20-40 μm size range. The temperature of air and particles are around 1100°C at a constant velocity of 70 m/s. The target coupon is made of Hastelloy X, a nickel-based alloy and the angle at which the particles impact the coupon varies from 30° to 80°. The experiments were performed with different amounts of total particle injected, concentration, and coupon angle to understand their effects on deposition. Similar research was carried out in the past at the same facility to study particle deposition at temperatures up to 1050°C and 70 m/s flow velocity. However, this previous research only studied how the coupon angle affects particle deposition; other parameters such as total particle input and particle concentration were not studied. It was found that particle deposition increases significantly at higher temperatures beyond 1050°C for higher coupon angle and amount of sand injected. Results from current study also show that deposition increases with increase in total sand injected, concentration, and coupon angle for a given temperature and velocity.

Acknowledgements

Dr. Wing Ng and Dr. Srinath Ekkad: Thank you for giving me an opportunity to work on this project, I could not have asked for better advisors and am very grateful for this. Working with you has not only enriched my research experience but also has been instrumental in my professional development, and for that I am forever grateful. Your insight and suggestions have helped me progress when the path forward was unclear.

I would like to give special thanks Dr. Jacob Delimont for teaching me everything about the project. Without his initial support, this work would not have been possible. Another special thanks to Andrew Boulanger for all the long hours and thoughtful discussions on this project in the past one year. A special thanks to Gus Paras and John Hutchison for their help in setting up the test rig. To Alan Arisi, David Mayo, John Gillespie, Kris Barboza, Prashant Singh, David Gomez, and Kartik Tyagi, I am very thankful to all of you for a variety of reasons. A special thanks to Diana Israel in the ME Dept. for personally placing several orders over past year and half. To James, Bill, Tim, Phil, and Johnny in the machine shop: Special thanks to everyone for your help in all the odd jobs and the formal ones.

I would also like to thank the Rolls Royce team: Brett Barker, Kwen Hsu, Paul Davis, and Bruce Varney for their guidance. This work would not have been possible without their support.

Finally, I would like to thank my mom Darshna and dad Dipan for all their love and support over the years.

All photos in this report are taken by the author unless specified otherwise.

Table of Contents

Abstract	ii
Acknowledgements	iii
Table of Contents	iv
List of Figures	v
List of Tables	vii
Nomenclature	viii
1. Introduction.....	1
1.1 Background	1
1.2 Past Studies	4
1.3 Objectives and Scope	7
2. Experimental Method.....	8
2.1 Aerothermal Rig.....	8
2.2 Instrumentation	14
2.3 Particles	15
2.4 Test Conditions	17
3. Data Reduction Method	18
4. Results and Discussion	22
4.1 Effects of Total Sand Injected on Deposition at Constant Temperature	22
4.2 Effect of Particle Concentration on Deposition at Constant Temperature and Total Sand Injected.....	25
4.3 Effect of Temperature on Particle Deposition at Constant Coupon Angle.....	26
4.4 Effect of Impact Angle on Particle Deposition at Constant Temperature	27
5. Conclusion	29
References	31
A. Appendix: APPL Building Modifications.....	33
B. Appendix: Aerothermal Test Rig Modifications.....	36
C. Appendix: Matlab Particle Counter Code	43

List of Figures

Figure 1. An example of V-22 Osprey operating at low altitude in particle-laden environment. .	1
Figure 2. Dominant mechanism for particle delivery in turbine vane with respect to particle diameter and velocity as summarized by Hamed et. al. [3]	3
Figure 3. VT Aerothermal Rig configured for restitution and deposition testing.	9
Figure 4. The main air supply to the Aerothermal Rig. Three pressure regulators bring down the pressure to a little over atmospheric and mitigate any upstream fluctuations.	10
Figure 5. Particle injection location in the aerothermal rig.	11
Figure 6. Particle injection system for the Aerothermal Rig.	12
Figure 7. CAD model of the test coupon orientation inside the test section. The support rod is connected to the rotatable flange at the top that can change coupon angle in increments of 10°.	13
Figure 8. This image shows coupon surface oriented at 90° with respect to the centerline of the equilibration tube.	14
Figure 9. MATLAB particle counter code counting locating individual particles from each image.	19
Figure 10. Microscopic image of particle deposition for 10g total sand injected at 200x zoom.	22
Figure 11. Microscopic image of particle deposition for 25g total sand injected at 200x zoom.	23
Figure 12. Microscopic image of particle deposition for 59g total sand injected at 200x zoom.	23
Figure 13. Particle deposition increases drastically when 59g sand is injected compared to lower sand amounts.	24
Figure 14. Particle deposition as a function of concentration. As the particle concentration increases, the particle deposition was also observed to increase linearly.	255
Figure 15. Particle deposition at temperatures ranging from 950°C to 1100°C at 30° coupon angle.	266
Figure 16. Particle deposition with respect to coupon angle at 1100°C temperature and 10g total sand injected.	28
Figure 17. Kaeser CS 75 compressor repurposed to supply shop air at APPL. The shed protects the compressor from rain and snow.	34
Figure 18. The pump for supplying cooling water housed in a repurposed shipping container. The container protects the pump from rain and snow.	35

Figure 19. The Aerothermal rig on rails at APPL. 37

Figure 20. Screenshot of LabVIEW VI with suggested changes. Additional thermocouples were mounted on the burner wall for monitoring purposes. 38

Figure 21. The fuel supply to the Aerothermal Rig is remotely controlled using the pneumatic valve and the particles are injected in to the rig through the particle hopper. 39

List of Tables

Table 1. ARD Test Dust Chemical Composition	16
Table 2. ARD Test Dust Size Distribution	16
Table 3. Test Matrix to Determine Factors Affecting Particle Deposition	17
Table 4. Calculation for number of images required for each test.	20

Nomenclature

ARD	Arizona Road Dust
x	Number of Particles per Image
\bar{x}	Sample Mean
n_i	Number of Sample Images
E	Margin of Error
Stk	Stokes' Number

Greek

σ	Standard Deviation
----------	--------------------

1. Introduction

1.1. Background

Operating gas turbine engines in particle laden environment can be detrimental to their performance. Ingested micro particles can significantly reduce the engine life and result in engine failure. Modern gas turbines are equipped with filters to prevent any foreign particles from entering. These filters are several feet tall and custom made for the environment in which the turbine is going to operate so that minimum amount of particles gets to the turbine. For example, a turbine operating in desert environment is equipped with sand filters to prevent it from entering. However, propulsive turbines generally do not have any filters due to space and weight constraints. Particles of all sizes and types can get ingested in such situations. Airplanes and helicopters with Vertical Take-off and Landing (VTOL) capability such as V-22 Osprey are subjected to high concentrations of microparticles when flying at low altitudes (See Figure 1). Gas turbine engines are subjected to environments that have particle concentrations as high as 2.17×10^9 particles per cubic meter [1]. Land-based turbines with air mass flow of 1000 lbm/s can ingest as much as 28,000 lbs of impurities in 8000 operational hours for particulate concentration of one ppmw [2].



Figure 1. An example of V-22 Osprey operating at low altitude in particle-laden environment.
[Dept. of Defense, Used under fair use, 2015]

Ingested micro-sand particles can deteriorate the engine performance in several ways. The primary mechanism of damage in the compressor (cold) section of the engine is erosion. Ingested particles erode the compressor blades resulting in its performance loss. Erosion damage in the compressor section can be characterized using coefficient of restitution (COR). COR indicates the amount of kinetic energy absorbed during a collision. It is calculated by taking the ratio of the kinetic energy of the particle after and before the collision. In the combustor section, the particulates could block the fuel injection nozzles resulting in improper combustion.

In the turbine section, the primary mechanism of damage is particulate deposition. Due to the high temperatures and velocities, the particles are easily deposited on the turbine blades and vanes thereby altering their aerodynamic profile. In many cases, the deposited particles block cooling holes or internal cooling passages on the turbine blades which results in blade material thermal damage.

Several studies have been conducted in the past to characterize particle deposition in gas turbine engines. Most of these studies consist of injecting micro-particles in a full-scale working turbine and then examining its effects afterwards [3,4]. Other studies have investigated particle deposition as a function of the test coupon angle, surface roughness, particle concentration, etc. [3,5]. These studies are empirical as there is no direct way to characterize particle deposition. The current study expands on the data available on empirical impact correlations by presenting sand deposition at its near melting temperatures. This will enable more accurate models and computational analysis of sand deposition in gas turbines.

There are many mechanisms through which sand particles are delivered inside gas turbine engines. The major mechanisms are (1) inertial impaction, (2) turbulent eddy diffusion, (3) Brownian diffusion, and (4) thermophoresis. Depending on the size of the particle, one of the deposition mechanisms will be dominant. Inertial impaction is dominant for particle size greater than 10 microns. This is because the particles have high momentum and do not follow deviating gas streamlines. This correlates with the Stokes number of the particles. The Stokes number of a particle states whether the particle will be able to respond to the change in flow. Because of momentum, the particles penetrate the flow boundary layer and ultimately impact with the airfoil. Particles smaller than one microns are affected by turbulent eddies in the surface boundary layer and are swept toward the airfoil and endwalls. This mechanism is referred to as turbulent eddy diffusion of particles. For Brownian diffusion, smaller particles interact with thermally agitated

gas molecules and impact randomly in the flow field. As for thermophoresis, particles of sizes ranging from 0.01 microns to 0.1 microns are driven from high temperature to low temperature regions. This is caused by boundary layer effects at the surface of the particle having a thermal gradient across it. These mechanisms for particle delivery have been summarized in Figure 2 shown below.

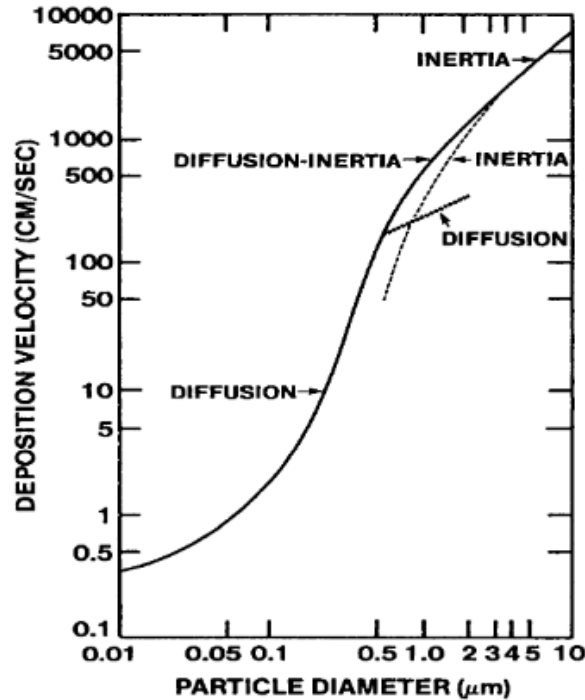


Figure 2. Dominant mechanism for particle delivery in turbine vane with respect to particle diameter and velocity as summarized by Hamed et. al. [Mechanism of particle delivery from Hamed, a., Tabakoff, W. C., and Wenglarz, R. V., 2006, “Erosion and Deposition in Turbomachinery,” J. Propuls. Power, **22**(2), pp. 350–360. Used under fair use, 2015].

Moreover, the London-van Der Waals force can also act on the particles near airfoil or endwall if they are electrically charged due to interaction with hot gases. As a result of this, smaller particles near the surface can get attracted towards it and ultimately deposit. If the above mentioned mechanisms are more dominant than the van der Waals force, the particle will rebound. If not, the particle will adhere to the surface.

Significant quantities of impurities can be delivered to the turbine airfoils due to the above mentioned mechanics. Typically, these impurities are of irregular shape and sizes. These particles are exposed to extreme flame temperatures when they pass through the combustor section. When

exposed to such extreme temperatures, the particles transform and are in molten state when they enter the turbine section. Depending on the sizes, the molten particles are delivered to various parts of the turbine section and deposit to the surface.

1.2. Past Studies

One of the earliest studies on particle deposition in gas turbines was published by Sieverding et al. [7] in the von Karman Institute handbook in which the authors highlighted that the three most important factors which effect deposition are (1) particle temperatures, (2) its type, and (3) size. Sieverding et al [7] also observed that the deposited particles can interact with each other, physically, depending on their concentration. Impacting particles interact with already deposited particles and in some cases, particles interact with each other in the flow stream if the concentration is very high. This phenomenon is even more prevalent in the extreme temperatures of hot gas path in a turbine and may result in alteration of their properties. Physical properties such as transition temperature are lowered for these particles. Transition temperature is the temperature at which the particle changes its state to molten. Friedlander and Sieverding [7,8] discussed that the melting temperature of ingested particles inside a gas turbine is significantly lower than their melting temperature in pure state. The lowering of the transition temperature is observed in all the particle types ingested in a gas turbine. Sand particles are complex mixtures of various crystalline solids that result in lowering of the melting temperature compared to individual particles' melting temperature. Dunn [3] studied various modes of failure in J-57, TF33, F100, F107, and F112 engines due to particle ingestion. The experiments were performed at Industrial Acoustics Engine Cell located at Edwards Air Force Base. The engines were exposed to different concentrations of impurities until they failed. The time taken for the engine to fail was recorded and it was found that engine fails early at higher concentration of impurities. It was concluded that higher concentration of impurities and properties of ingested particles are important factors in particle deposition.

Kim et al. [4] performed deposition tests on a hot section test system experimental test rig made from Pratt and Whitney F-100 and Allison T65 engine components. Deposition at particle concentrations of 250, 500, and 1000 mg/m³ was tested in this study. The turbine inlet temperatures

ranged from around 1050°C to 1250°C. Deposition was characterized by measuring the deposited mass of particles. It was found that deposition increased linearly with increase in dust concentration. It was also found that location of particle deposits is strongly influenced by whether or not they are able to follow the flow.

Jensen *et. al.* [2] performed deposition tests using sand particles on an accelerated deposition testing facility on a nickel super alloy coupon. The tests were performed at coupon angles ranging from 30° to 90° and flow temperature of 1150°C. It was found that deposition increased with increase in coupon angle. On the same testing facility, Crosby *et. al* [5] performed accelerated tests simulating 8000 hours of turbine service. It was found that particle deposition is higher for coupons with higher surface roughness. This means that more particles were captured by the surface compared to a relatively smoother surface.

This phenomenon of particle deposition on impact was explained by Smeltzer *et. al.* [9]. It was proposed that when the particles impact on the metal surface in the extreme conditions of a turbine, they stagnate momentarily and impart some kinetic and thermal energy to the metal. This causes localized heating of the particles and the impacting surface at their point of contacts. The localized heating is enough to melt the particle and the impacting material around the region of impact and bind to the metal surface. The metal surface is relatively cooler due to its cooling mechanisms and aids in forming a permanent bond with the particles. If the particles are impacting the metal surface in molten state, the impact will generate enough energy to locally melt the metal. This bonds the molten metal and impacting particles and ultimately results in their deposition.

Walsh *et. al.* [10] studied particle deposition on film-cooling holes of a turbine vane. The experiments were performed on test coupons with various cooling hole geometries at temperatures ranging from room temperature to approximately 1000°C. The deposition was characterized using a flow parameter across the film cooling hole. It was found that particle deposition increased significantly at around 1000°C. It was concluded that particles most likely melted on impact and adhered to the surface. This concurs with Smeltzer and Sieverding regarding lowering of melting temperature of particles [7,9].

To understand how much energy is being imparted on to the metal surface and particle during impact, COR studies were performed by Reagle and Delimont [11,12] using Arizona Road Dust. The experiments were performed on VT Aerothermal Rig at temperatures ranging from room temperature to 1050°C. It was found that COR decreases at higher coupon angles. This means that

more energy is absorbed by the blade material during impact at higher coupon angles. Impacting particles lose more energy to the metal surface resulting in higher localized temperatures and deposit. Delimont et al. [12] also found that particle deposition onsets at around 1000°C and measured deposition at various particle coupon angles. It was found that particle deposition increases with increasing test coupon angle relative to the air flow. The deposition is even more severe when the particles are at its near melting temperatures. This shows that flow temperature and COR has direct impact on particle deposition.

In order to understand the particle deposition types, Borom *et. al.* [13] performed an electron microprobe analysis on gas turbine components damaged by sand particulates. In most of the cases, oxides of silicon, calcium, magnesium, and aluminum (CMAS) deposited onto the turbine section airfoil surfaces. Oxides of CMAS are the most common compounds found in sand and ash. Similar analysis was performed by Smialek *et. al.* [14] on damaged helicopter engines operating in the Middle East and found that oxides of CMAS were the primary component of the deposited material. Crosby et al. [15] performed accelerated tests on a bare metal coupon at 1150° flow temperature and 45° coupon angle. Scanning electron microscope analysis was performed to find elemental composition of deposits formed by ash. The composition of the deposited material was found similar to that of Smialek and Borom [14,16].

Based on phase equilibria diagrams given by Sieverding [7] and Maier et al. [17], it is found that the melting temperature of CMAS mixture is lower than the melting temperature of the individual particles. The lowering of the temperature depends on the composition of each oxides present in the mixture.

Deposition has not been documented during its initial onset at near melting temperatures of crystalline sand particles. More study is needed before particle transport and energy transfer mechanisms of the ingested particles can be confidently included in the computational models. This study provides further insight into particle deposition as a function of temperature and impact angle and will help narrow the gap. The companion works for this study [12,18] investigate the effects of temperature and impact angle at lower temperatures. The results from these studies provide insight into particle deposition at near melting temperatures and could be used for validation purposes.

1.3. Objectives and Scope

The objective of this study is to determine the effects of temperature and total sand injected on deposition at constant impact velocity. The test coupon on which experiments are performed is made from a high temperature nickel super alloy, Hastelloy X. The experiments are performed at 30°, 50°, 80°, and 90° impact angles at a constant velocity of 70 m/s. From previous studies [6,11,12], it was found that particle deposition increases as temperature increases.

From previous research [2,6,7,12], the melting temperature of sand is around 1050°C. This study tests sand deposition at temperatures up to 1100°C. It is expected that with increase in temperature, a sharp increase in deposition will occur.

This study also investigates the effects of particle concentration on deposition at temperatures up to 1100°C. Based on previous research [3,19], particle deposition should increase with higher particle concentration. This study hopes to add on to the data obtained previously and also look into other parameters that affect particle deposition.

2. Experimental Method

The experiments are performed on Virginia Tech Aerothermal Rig for this study. This section briefly explains the aerothermal rig and its current capabilities. Detailed explanation on the aerothermal rig is given by Delimont et. al [12].

2.1. Aerothermal Rig

The Aerothermal Rig was donated by Rolls-Royce to Virginia Tech in 2010. It was previously installed in Indianapolis, Indiana, for heat transfer studies by Nealy *et al.* [20] and Hylton *et. al.*[20]. The original operation specifications for this rig were reported by Rolls Royce as air flow rate of 2.2 kg/s at a maximum pressure and temperature of 16 atm and 2033 K, respectively.

The current test rig has been explain in detail by [8, 9] and has been described here briefly. The rig has been modified from its original configuration to allow sand to be injected immediately downstream of the burner. Figure 3 is an image of a CAD model of the VT Aerothermal Rig showing its layout in the current configuration. The rig was used previously by Delimont et al [12] to study sand ingestion at temperatures lower than 1050°C. Since the work by Delimont et al., the equilibration tube has been changed to allow for a higher maximum operating temperature. The current maximum test section temperature of the rig is 1100°C.

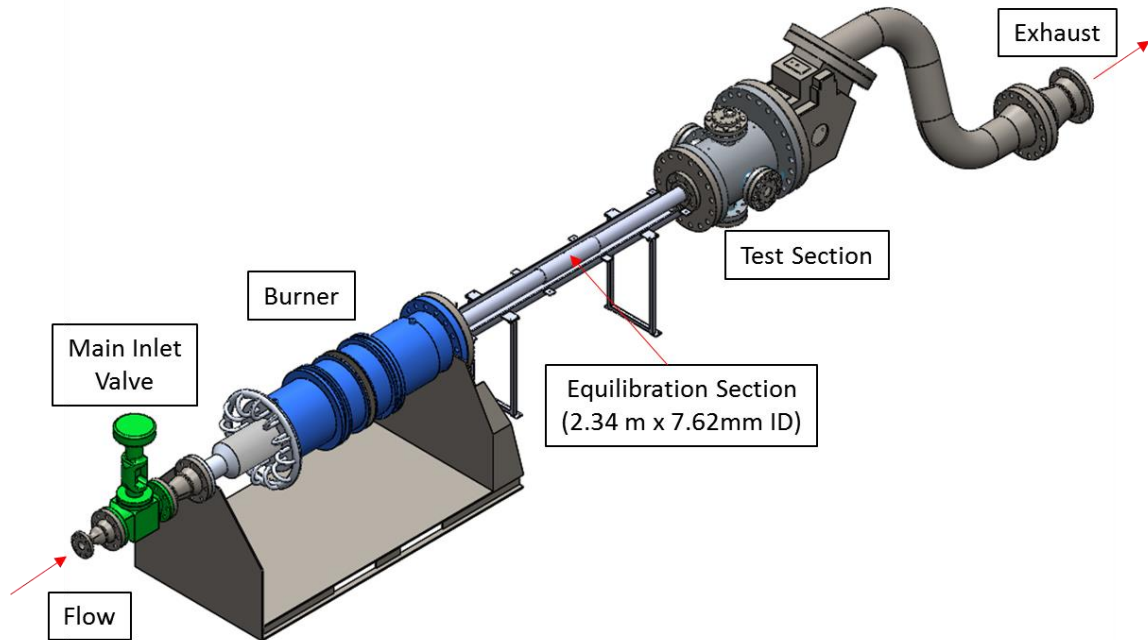


Figure 3. VT Aerothermal Rig configured for restitution and deposition testing.

A compressor supplies compressed air to a main buffer tank at a maximum mass flow rate of 0.16 kg/s. The main buffer tank is connected to a smaller secondary buffer tank inside the test cell to mitigate any pressure fluctuations. The air from the secondary buffer tank goes through a series of regulator valves that control the flow rate of the air before it goes through the main control valve. The main inlet control valve is used to make finer adjustments to the air flow going into the test rig. The regulator control valves are adjustable so that constant mass flow rates can be maintained for values lesser than 0.16 kg/s. These regulators allow precise control over mass flow rates of air into the rig, which results in independent control over temperature and velocity. Figure 4 displays a picture of the regulator valves used in the VT Aerothermal Rig. The airflow passes from the secondary buffer tank to the regulators, then to the main control valve. The regulators are arranged in U-shaped due to space constraints. A pitot-static probe, pressure transducer, and a thermocouple instrument the flow just before it exits to the test rig. These instruments are connected such that the flow is fully-developed before reaching them. The instruments are connected at about 30 inches from the second 90 degree turn in the piping.

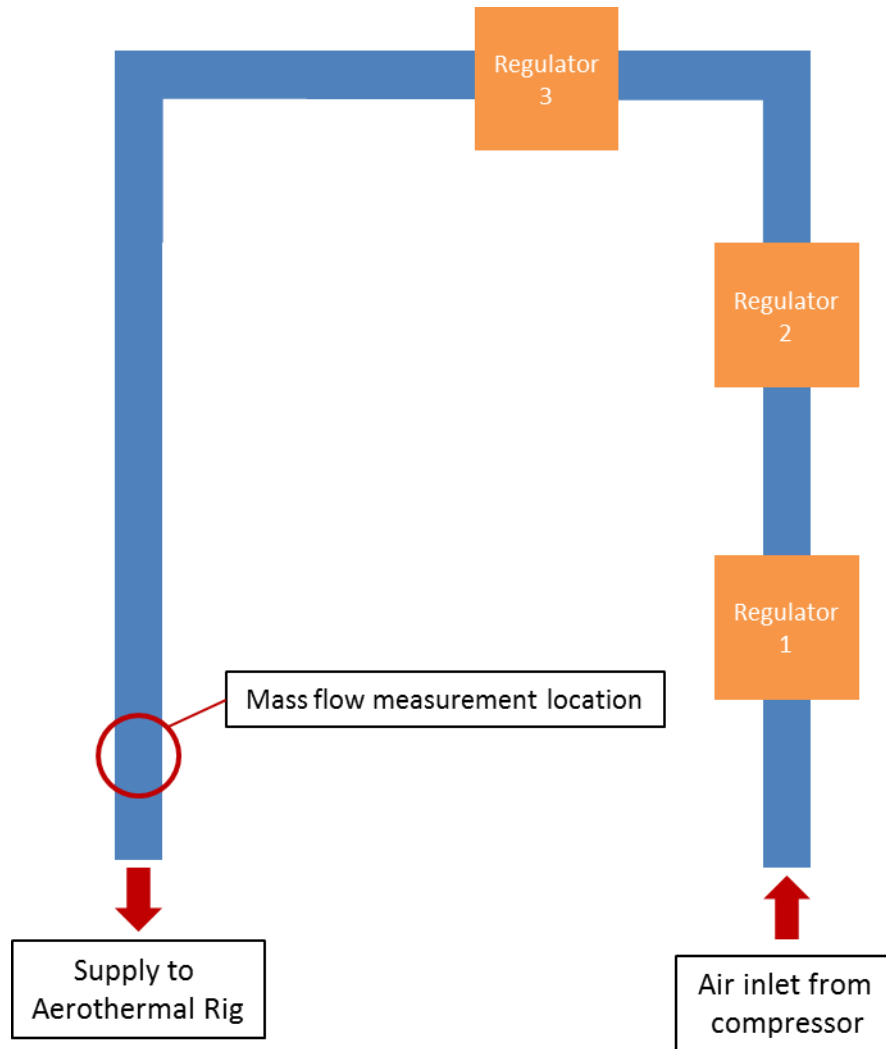


Figure 4. The main air supply to the Aerothermal Rig. Three pressure regulators bring down the pressure to a little over atmospheric and mitigate any upstream fluctuations.

After passing through the control valve, the air enters the sudden-expansion, water-cooled burner that heats the flow using methane as fuel (See Figure 3). The sand particles are injected into the main flow after the burner. Figure 5 shows the particle injection location on the aerothermal rig. The particles are injected in the opposite direction of the main air flow to allow for proper mixing. Moreover, the particles are injected right after the burner so that they have enough time to reach the main air flow temperature and velocity.

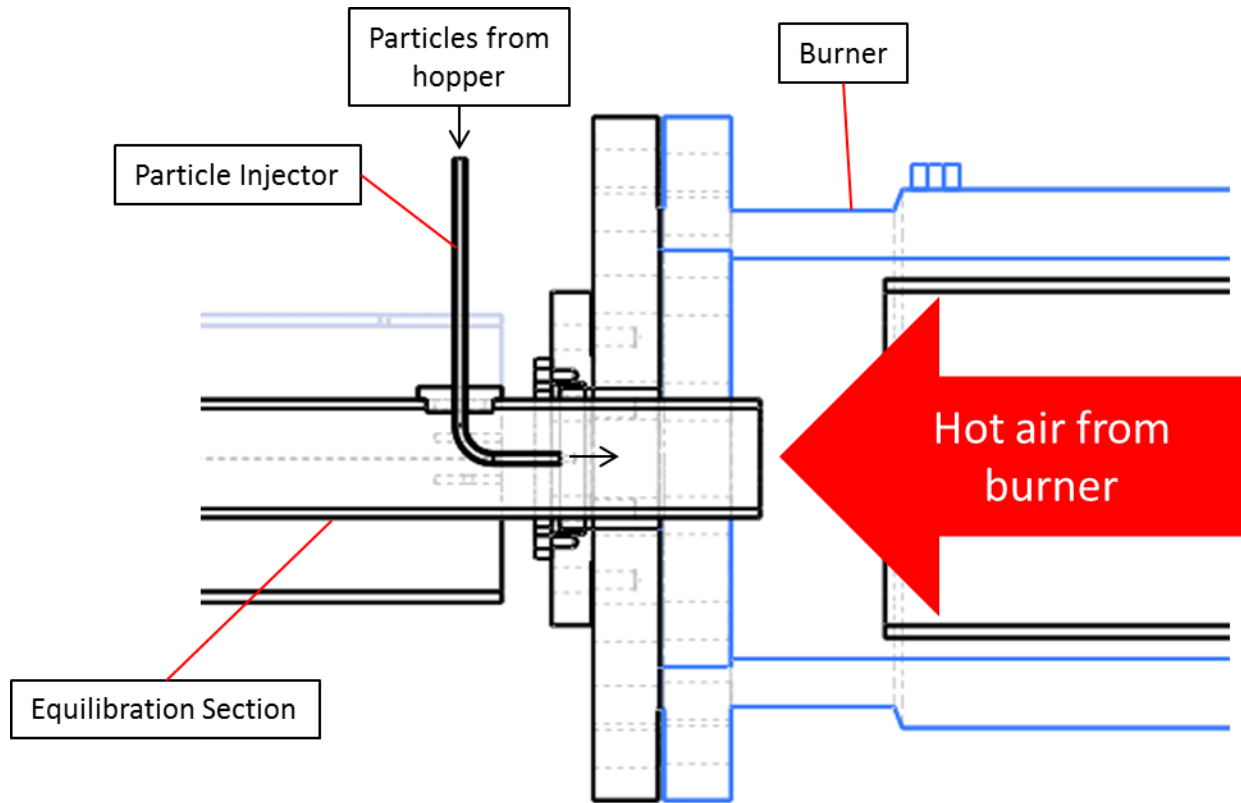


Figure 5. Particle injection location in the aerothermal rig.

The particles are injected into the test rig using a particle hopper. The hopper consists of a vertical steel pipe connected to a wye fitted with a ball valve. A pneumatic vibrator is attached to the vertical pipe which vibrates with air supply. The vertical pipe is also connected to air supply from the top. There is bleed air from the secondary buffer tank always going through the wye fitting into the test rig. When signal is given from the LabVIEW program, solenoid valves activate and supply air to the vibrator and the steel pipe. The ball valve is kept slightly open. This allows for the sand particles to drop at a constant rate in the bleed air stream. The particles are then carried into the test rig through the bleed air. Figure 6 shows the particle injector setup.

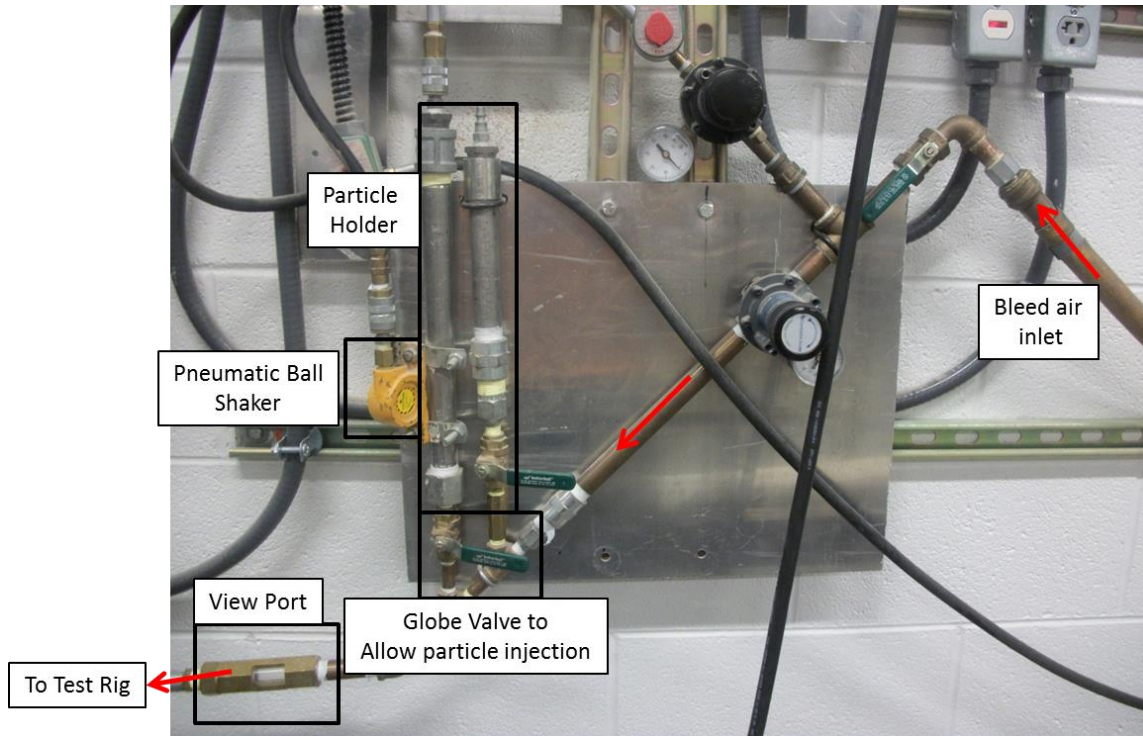


Figure 6. Particle injection system for the Aerothermal Rig.

The air travels through the 7.62 cm diameter, 2.34 m equilibration tube to allow the sand particles to reach the temperature and velocity of the air flow. The flow then exits the equilibration tube as a free jet into the test section and impinges on the test coupon. During each test, sufficient time is allowed for the temperature of the rig to reach equilibrium before sand particles are injected and measurements of the particles are taken.

A CAD image of the test section without the outer casing walls is shown in Figure 7. The figure shows the test coupon support that can be rotated in 10° increments. This allows for various angles of impingement to be studied. The dimensions of the test coupon on which the particles are impacted are 3.81 cm by 6.35 cm. The coupon is rectangular in shape to allow for sufficient area to be projected normal to the flow when testing at shallow impingement angles. Before each test, the coupon is polished to a mirror finish with a measured RMS roughness less than 0.2 microns to ensure surface roughness effects are minimized.

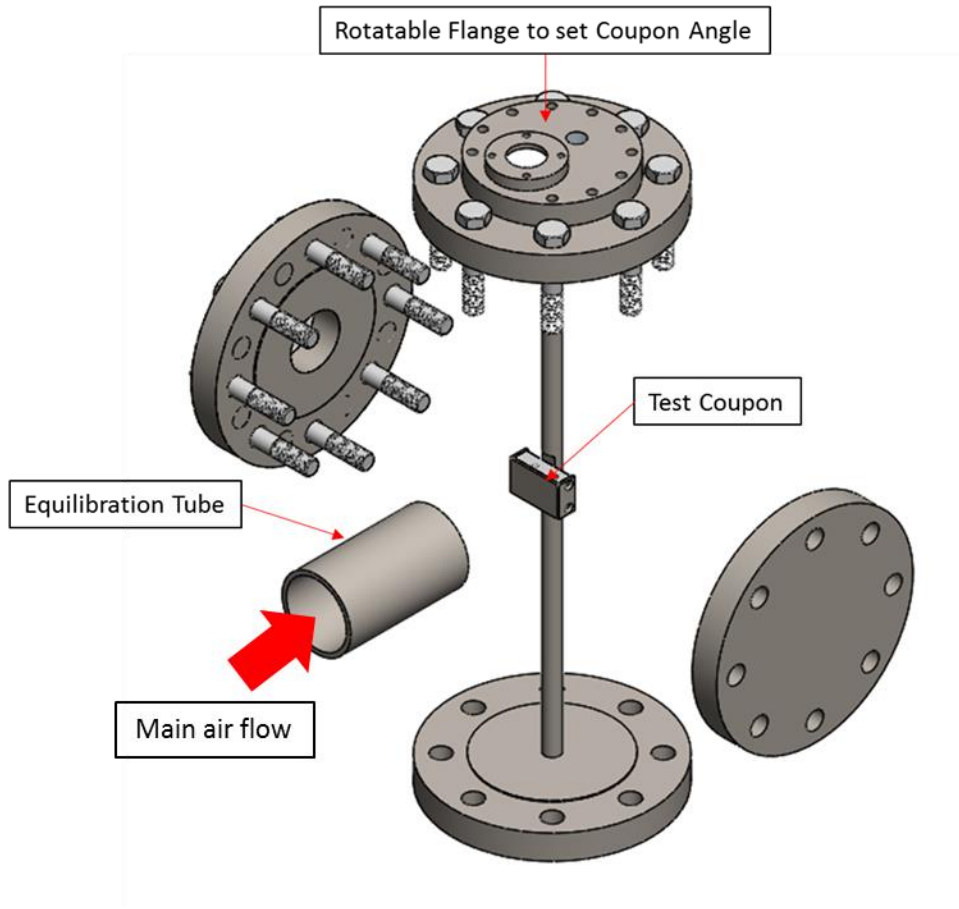


Figure 7. CAD model of the test coupon orientation inside the test section. The support rod is connected to the rotatable flange at the top that can change coupon angle in increments of 10° .

Figure 8 below shows the orientation of coupon with respect to the main flow which defines the coupon angle. The coupon angle is defined as the angle between the centerline of the equilibration tube with respect to the surface of the coupon. In figure 8, the coupon angle is 90° . Rotating the coupon clockwise or counterclockwise will lower the coupon angle.

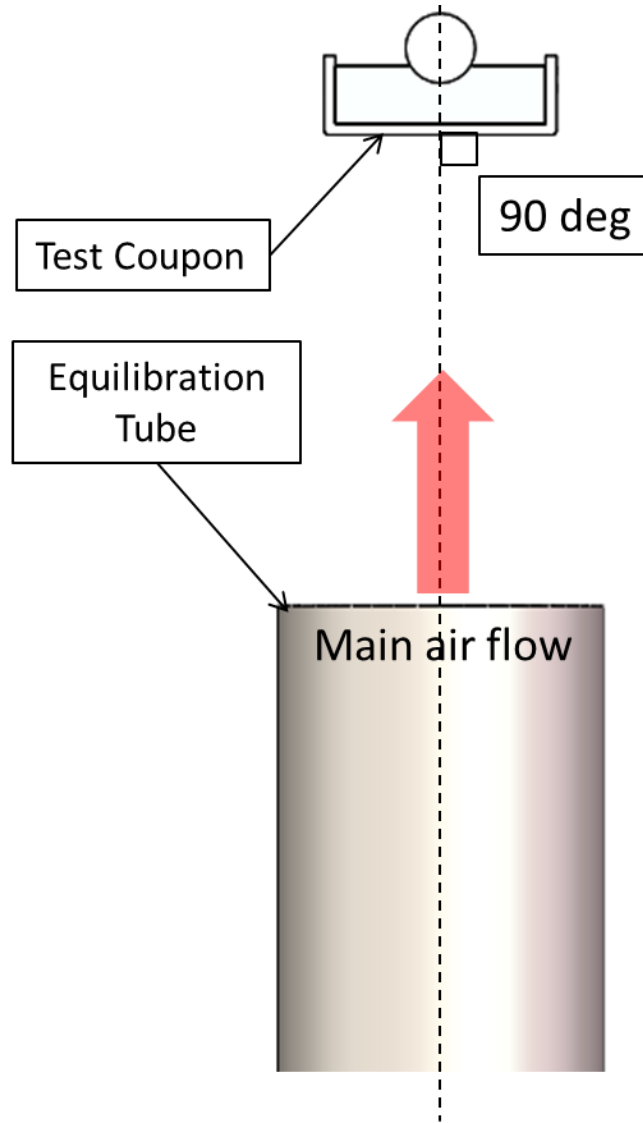


Figure 8. This image shows coupon surface oriented at 90° with respect to the centerline of the equilibration tube.

2.2. Instrumentation

A traversing Pitot-static probe is mounted at the exit of the equilibration tube to measure the exiting flow velocity. Because the probe is mounted to a traverse mechanism it can be placed in the flow to verify test conditions prior to the run and then removed so that it is neither damaged nor clogged by sand while particles are being injected into the flow. The probe is moved out of the test section during particle injection. Detailed information on the Pitot-static probe survey is given by Delimont *et. al.* [12].

To measure the temperature of the air exiting the equilibration tube, a K-type thermocouple is placed at the top of the coupon. Additionally, a thermocouple is buried inside the metal of the coupon back plate support, sealed with high temperature ceramic adhesive to get a rough estimate of the coupon temperature. There are many other thermocouples that are also placed on and inside the rig. These thermocouples are used to ensure that the rig has reached equilibrium temperature and to make sure that the rig does not go over its safe operational limits.

A high resolution camera is used to monitor particle injection and is configured to provide a live feed of the window port downstream of the particle injector to a computer or a smart phone. The resolution of the live feed is 720p and has a lag of one second. The camera is used to measure the time it takes for the particle injector to empty allowing for the sand concentration to be calculated during each test.

2.3. Particles

The sand particles used for this test are Arizona Road Dust (ARD). The particle size of the ARD used for this test was a size range of 20-40 μ m. The mean size is 26.71 μ m by volume for this size range. The numerical mean particle size was calculated from particle batch analysis provided by the particle manufacturer of the ARD used in the experiments. A narrow size range of particles is extremely important so that the possible effects of particle size do not contaminate the test results. In actual conditions, particles of all sizes are ingested into the engines. However, for simplicity purposes the selected size range will minimize any effect due to particle size on the results. The chemical composition as well as description of particle size distribution of this test dust range is reported in Table 1 and Table 2 as provided by the manufacturer, Powder Technology Inc. The chemical composition reported is the bulk chemical composition of the ARD but individual particles will vary in composition.

Table 1. ARD Test Dust Chemical Composition

Chemical	% Weight	Melting Point (K)
Quartz (SiO ₂)	68-76	1983
Aluminum Oxide (Al ₂ O ₃)	10-15	2323
Iron Oxide (Fe ₂ O ₃)	2-5	1838
Calcium Oxide (CaO)	2-5	2845
Potassium Oxide (K ₂ O)	2-5	1013
Sodium Oxide (Na ₂ O)	2-4	1548
Magnesium Oxide (MgO)	1-2	3073
Titanium Dioxide (TiO ₂)	0.5-1	3116

Table 2. ARD Test Dust Size Distribution

Particle Size (µm)	Cumulative Percent Volume (%)
<15.10	<1.16
<29.25	<50
<40.91	<99.04

Small microparticles may clump together during storage due to moisture. This can skew the results as clumped particles can interact physically during testing. In order to avoid this and achieve accurate test results, the sand is heated for several hours to remove moisture from the particles. This prevents particles from clumping and reduces any possibility of error in testing that would occur otherwise.

2.4. Test Conditions

Prior experiments [11,12] on this rig had maximum temperatures of 1050°C at 70 m/s flow velocity. Same amount of sand was used in these studies. The current study examines the effect of particle deposition at 1100°C at 70 m/s flow velocity. Different amounts of sand was used in this study to understand the relationship between total sand injected and deposition. The coupon back plate temperature is lower than the air and particle temperature. This is due to the conductive losses through the support rod and radiative losses inside the test section. Table 3 shows the experimental condition and test matrix. The experimental conditions are chosen based on results obtained by Delimont et al. [12], Walsh et al.[10], and Crosby et al [15]. Performing these experiments will provide insight in to effect of total sand injected, coupon angle, particle concentration, and temperature on deposition. An additional run was performed at 1050°C and 50° coupon angle to verify the repeatability of the data. It was found that data was repeatable within 2 particles per mm² for the same experimental conditions conducted by Delimont et al. [12].

Table 3. Test Matrix to Determine Factors Affecting Particle Deposition

Air Temperature (°C)	Coupon Angle (degree)	Total Sand Injected (g)	Particle Concentration (ppmw)
1100	30	10, 59	4500, 10000, 22000
	50	10, 25, 30, 59	10000
	80	10, 59	10000
	90	10, 59	10000

3. Data Reduction Method

Quantifying particle deposition is a complex problem as it depends on particle size, shape, concentration, temperature, velocity, angle of impact, etc. There is no proper way to characterize deposition as some of these parameters could be difficult to measure in a gas turbine. Hence, researchers have developed their own techniques to characterize particle deposition in laboratory experiments. Walsh et al. [10] defined a flow parameter characterized deposition in film cooling holes. The flow parameter characterizes deposition based on the decrease in coolant mass flow through the cooling hole. Crosby et al. [5] characterized microparticle deposition by reporting changes in surface roughness of the test coupon at different intervals during the test. Delimont et al. [12] characterized microparticle deposition by measuring the number of particles deposited per sq. mm. on the surface of the test coupon. The current study also characterizes particle deposition by measuring the number of particles deposited per sq.mm of the test coupon surface area. The deposition images on the coupon are taken using a Zeiss Vert.A1 microscope equipped with AxioCam MRc 5 camera. The images taken using the microscope can be scaled (pixels to distance). The scale is automatically calibrated according to the magnification of the microscope.

Knowledge of particle density over the entire coupon surface will provide the most accurate result. However, taking microscopic images of the entire surface is impractical. In order to solve this issue, the number of images required to represent the true particle density is determined statistically. The technique used is developed by Cochran [21] and is summarized by Bartlett *et al.* [22]. This technique is heavily dependent on the confidence interval and desired margin of error. These two parameters are selected by the researcher depending on the type of study. For the current study, Z-value for 95% confidence interval and estimating error as 10% of the mean of deposited particles in the initial sample for margin of error are used. These parameters are chosen as they provide precise results without taking huge number of sample images of the coupon surface. Initially, 15 microscopic images are taken from leading edge to the trailing edge of the coupon along the centerline. The particle deposition is higher for all coupon angles at the leading edge and then decreases towards the trailing edge. Taking images along the length of the coupon will cover all range of deposited particle densities on the surface. The images are processed using a MATLAB code that gives number of particles deposited per image as shown in Figure 8.

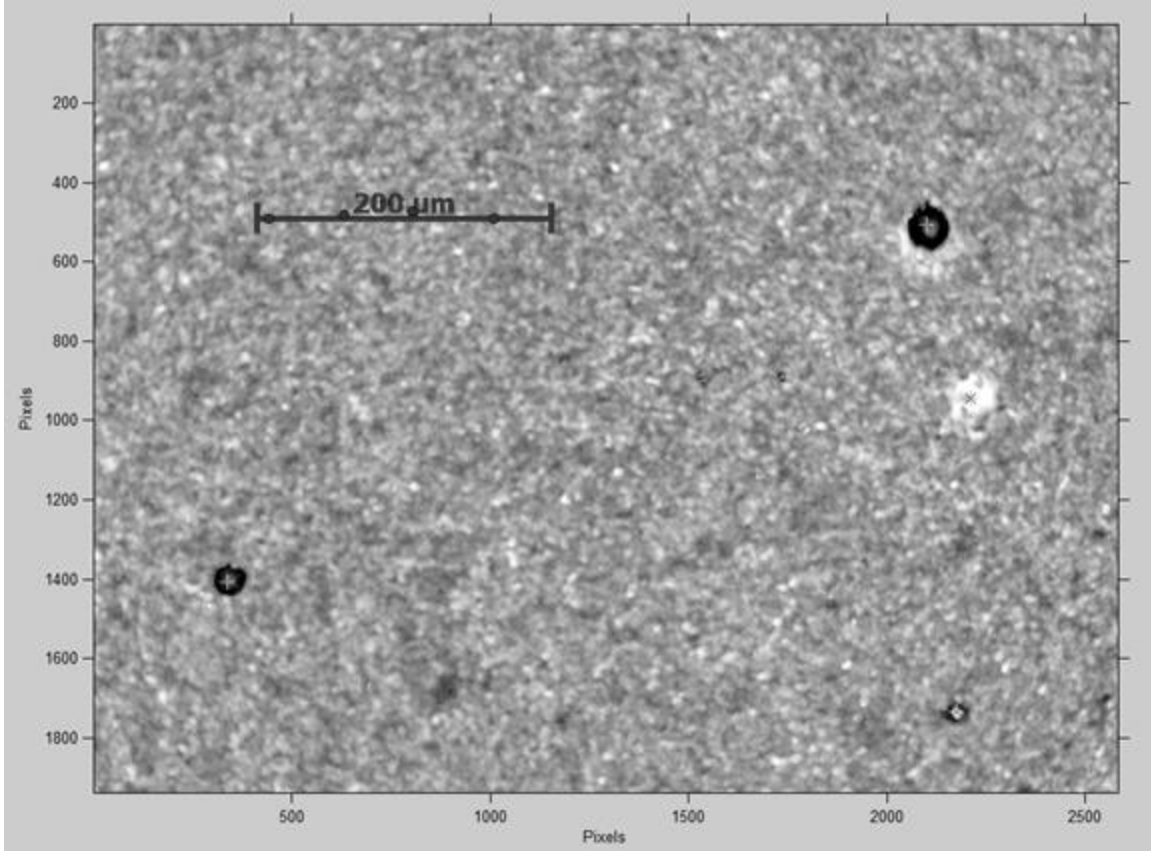


Figure 9. MATLAB particle counter code counting locating individual particles from each image.

Once the number of deposited particles is known in each of the 15 images, the standard deviation of the particles is calculated as:

$$\sigma = \sqrt{\frac{\sum(x - \bar{x})^2}{n_i}} \quad (1)$$

Here, σ is the standard deviation, x is the number of particles per image, \bar{x} is the mean of the sample, and n_i is the total number of images. The standard deviation will dictate the number of images (samples) needed to represent the overall deposition within a desired interval. The total number of images needed can be calculated as follows:

$$n = \left[\frac{\sigma * z_{\alpha/2}}{E} \right]^2 \quad (2)$$

where, n is total number of images needed to represent particle deposition over the coupon surface, E is the allowed margin of error in number of particles per image and is kept at 10% of the mean calculated from the initial samples. $z_{\alpha/2}$ is the statistical z-score.

At lower coupon angles, more particles are deposited at the leading edge than at the trailing edge. Due to this, the standard deviation is relatively high compared to standard deviation at higher coupon angles. This means that more images would be required at lower coupon angles to properly represent average particles deposited over the entire surface area. The standard deviation and number of images taken in each experiment is given in Table 4 below.

Table 4. Calculation for number of images required for each test.

Temperature (°C)	Velocity (m/s)	Total Sand Injected (g)	Coupon Angle (°)	Standard Deviation	Number of Images
1100	70	10	30	4.62	20
		10	50	3.77	14
		10	80	5.01	24
		10	90	3.69	13
		10	30	8.21	29
		10	30	5.29	27
		25	50	9.87	42
		30	50	5.61	30
		59	50	9.27	37
		59	30	12.78	39

Additional images are taken along the centerline of the coupon to meet the calculated number of images requirement. These images are then again processed using the MATLAB particle counter code and number of deposited particles in each image is measured. Each image is

2584*1986 pixels and the calibration factor from pixels to mm is (3700 pixels/1 mm) automatically provided by the microscope. This ratio is then used to calculate number of particles deposited per sq.mm. on the coupon surface for each image as shown in equation 3 below. Finally, average number of deposited particles are calculated from each of the calculated particles per sq.mm. for each image.

$$\frac{\text{Number of Particles}}{\text{mm}^2} = \frac{\text{Number of Particles}}{2584 * 1986 \text{ pixels}^2} * \left(\frac{3700 \text{ pixels}}{1 \text{ mm}}\right)^2 \quad (3)$$

4. Results and Discussion

4.1 Effects of Total Sand Injected on Deposition at Constant Temperature

Three experiments are performed for coupon angle of 50° at flow temperature and velocity of 1100°C and 70 m/s . The experiments were performed using ARD at three different amounts of sand: 10g, 25g, and 59g. Microscopic images of the deposited particles were taken post experiment. Figures 9-11 show microscopic images of the coupon taken after the experiment. In the images, many particles are out of focus as they are protruding out of the focal plane of the microscope.

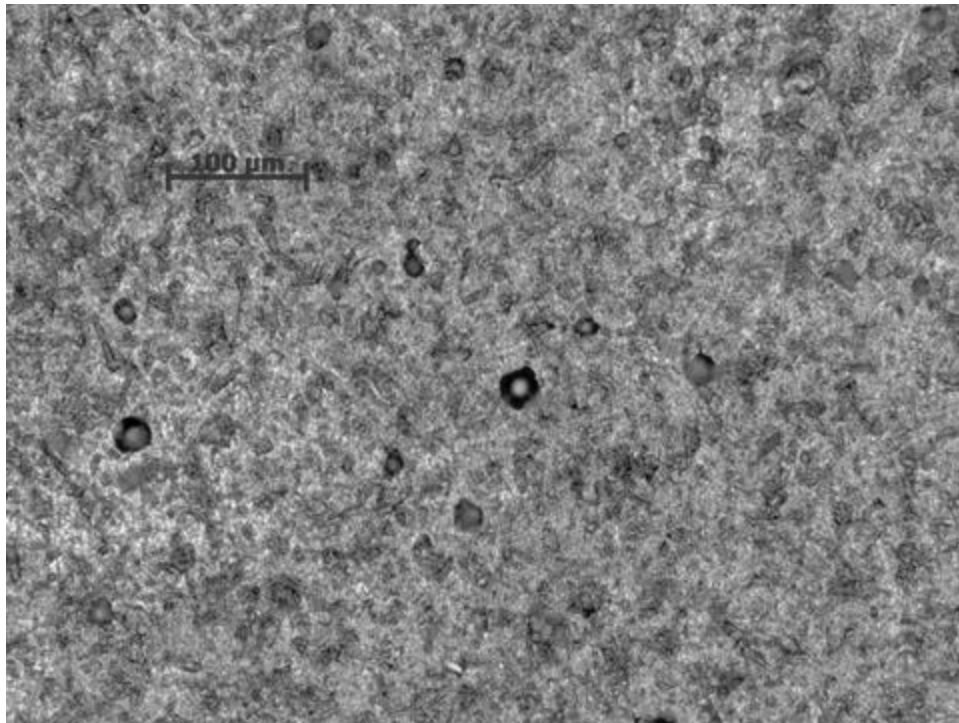


Figure 10. Microscopic image of particle deposition for 10g total sand injected at 200x zoom.

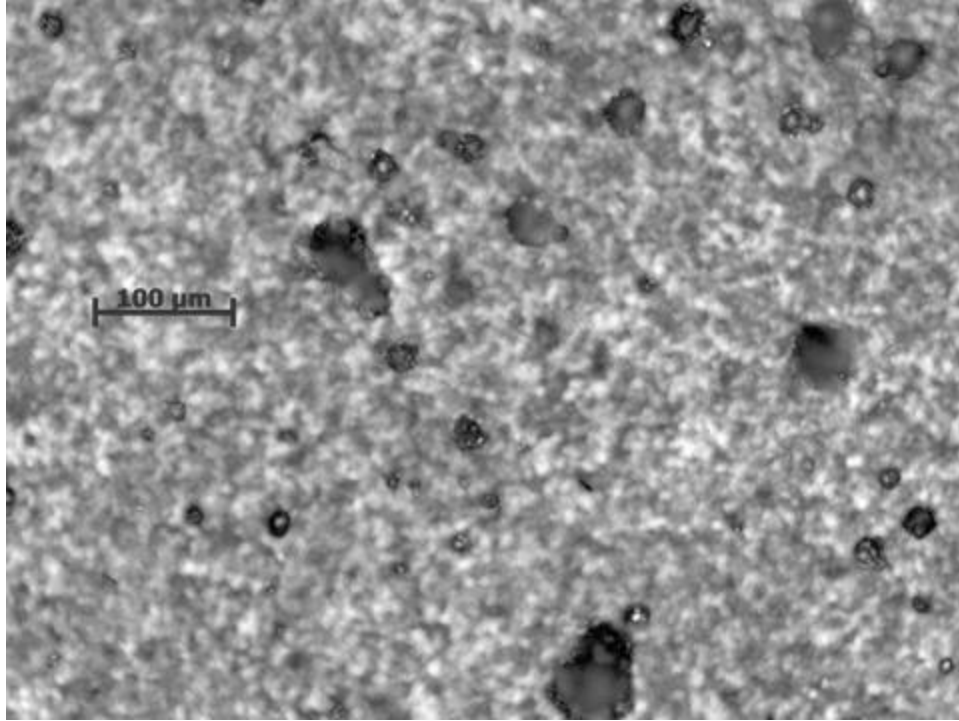


Figure 11. Microscopic image of particle deposition for 25g total sand injected at 200x zoom.

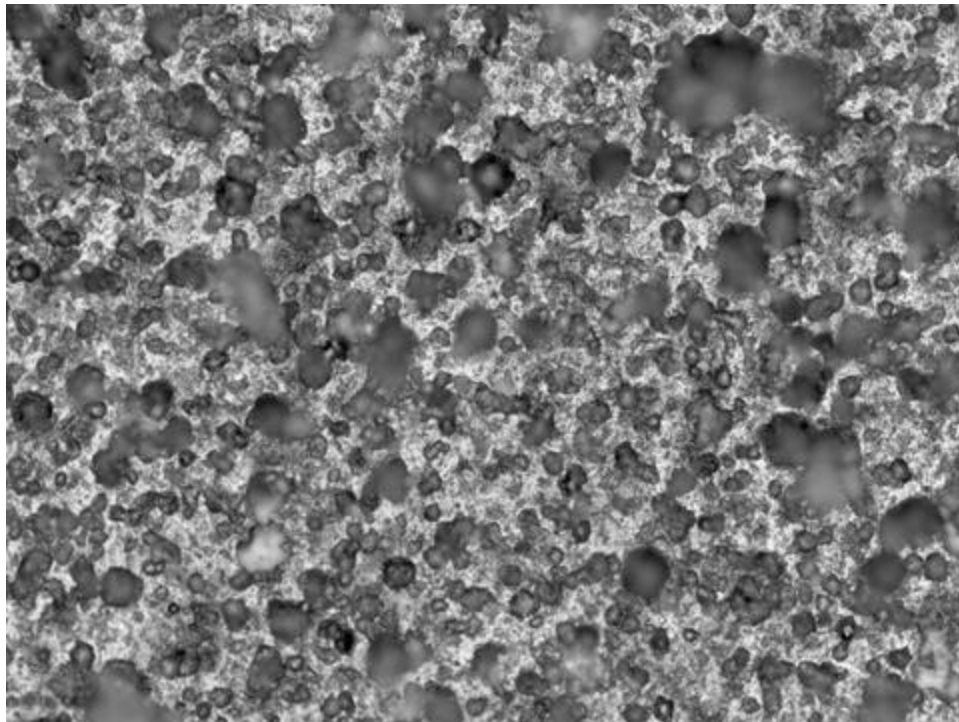


Figure 12. Microscopic image of particle deposition for 59g total sand injected at 200x zoom.

It was found that total sand injected and particle concentration have a significant effect on deposition. Figure 12 shows particle deposition as a function of total sand injected at 50° coupon angle, 1100° C flow temperature, and 70 m/s flow velocity. These experiments were performed at a constant particle concentration of ~10000 ppmw.

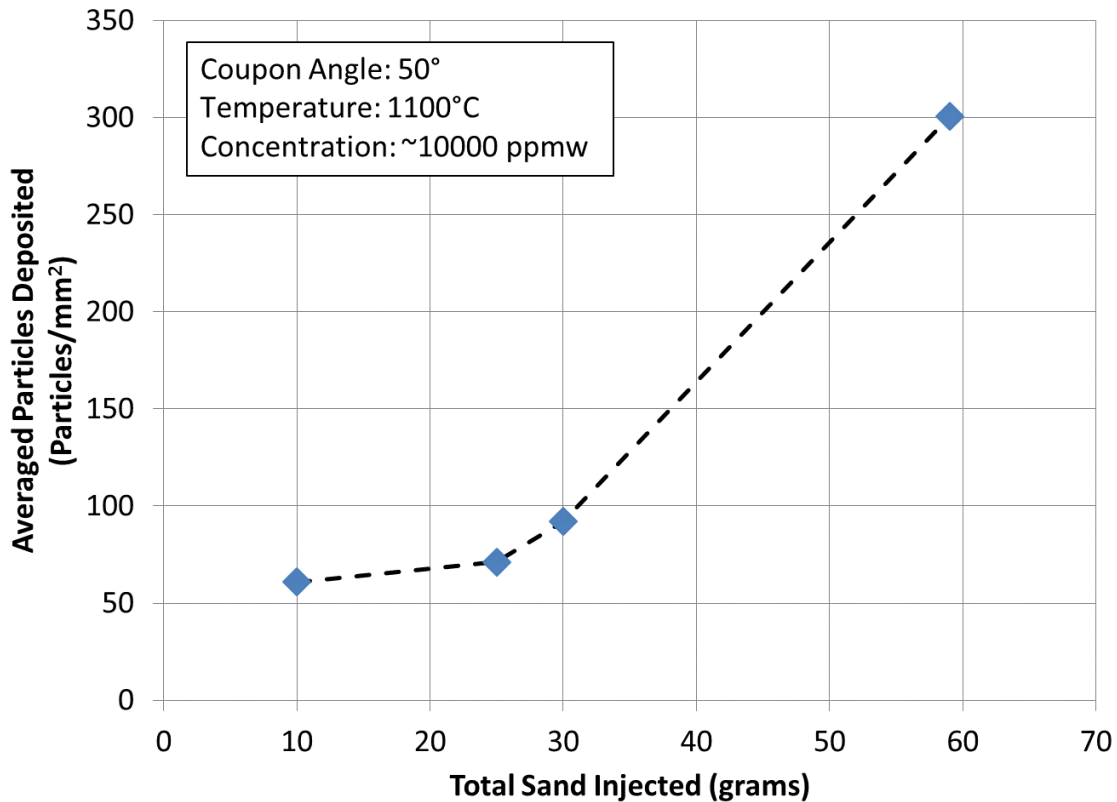


Figure 13. Particle deposition increases drastically when 59g sand is injected compared to lower sand amounts.

As can be seen from Figure 12, deposition increases drastically when more sand is injected. Once the deposition begins, the surface roughness increases, which increases the probability of particles sticking to the surface. Moreover, once the deposits starts forming, the incoming sand starts impacting on the particles deposited initially instead of the coupon metal (See Figure 11). This can lead to interaction between the already deposited particles and the incoming particles which results higher rate at which particles deposit on the surface [7,23].

4.2 Effect of Particle Concentration on Deposition at Constant Temperature and Total Sand Injected

Three additional experiments were performed to observe deposition as a function of particle concentration. Particles were injected with different valve openings and bulk concentration rate was calculated based on total amount of sand injected during the test and total time taken for all the particles to inject. The valve was cracked open using a space gage to ensure repeatability of particle concentration in the mail flow. The experiments were performed at 30° coupon angle, 1100° C flow temperature, and 70 m/s flow velocity. The particles were injected approximately at 0.6 g/s, 1 g/s, and 2.2 g/s. The particle concentration was around 5300 ppmw, 10,000 ppmw, and 22,000 ppmw. All three experiments were performed using 10 g of sand. The results obtained from these experiments are shown in Figure 13 below.

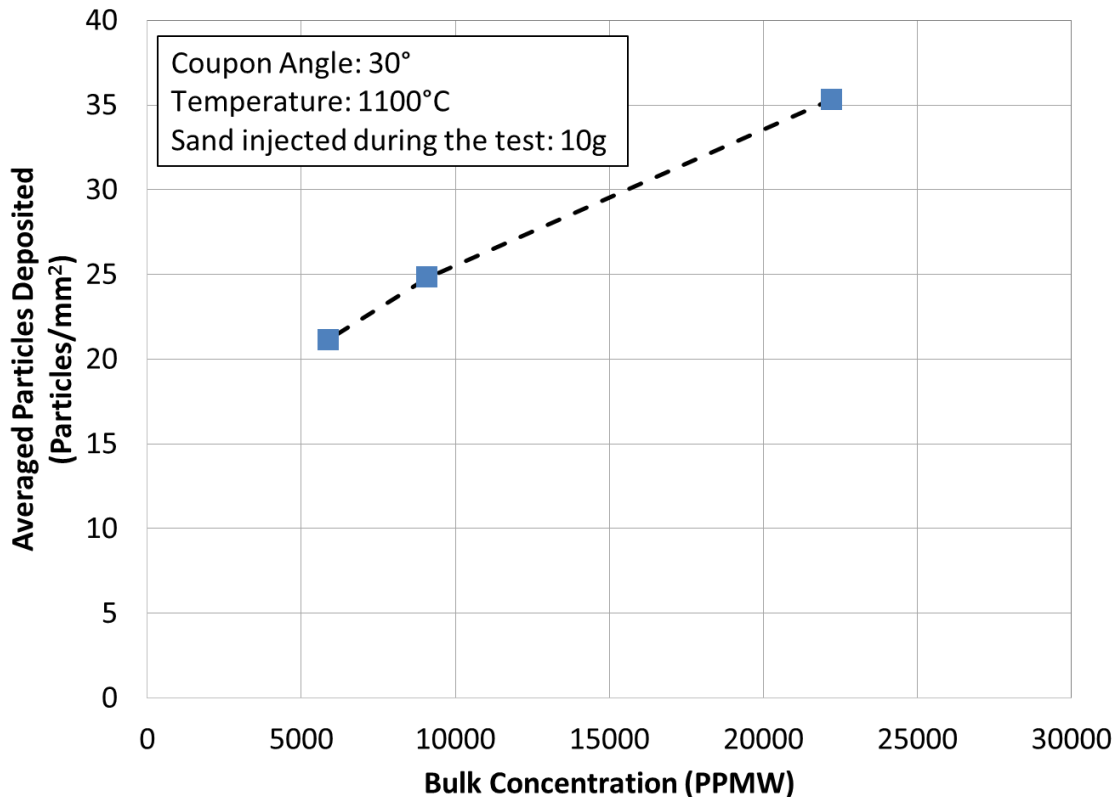


Figure 14. Particle deposition as a function of concentration. As the particle concentration increases, the particle deposition was also observed to increase linearly.

This increase in deposition is likely caused by interaction of particles with each other in the flow. These particles interact with each other physically resulting in change of physical properties such as lowering of melting temperature [7,10,23]. This can result in higher deposition.

4.3 Effect of Temperature on Particle Deposition at Constant Coupon Angle

Moreover, additional experiments were performed at 30° and 50° coupon angles and 1100°C flow temperature with 59g total sand injected. The experimental conditions were kept the same as [8, 9]. Figures 14 and 15 show particle deposition at temperatures ranging from 950°C to 1100°C at 30° and 50° coupon angle. Deposition at 950°C, 1000°C, and 1050°C were performed by Delimont et al. [12,18] and are used for comparison.

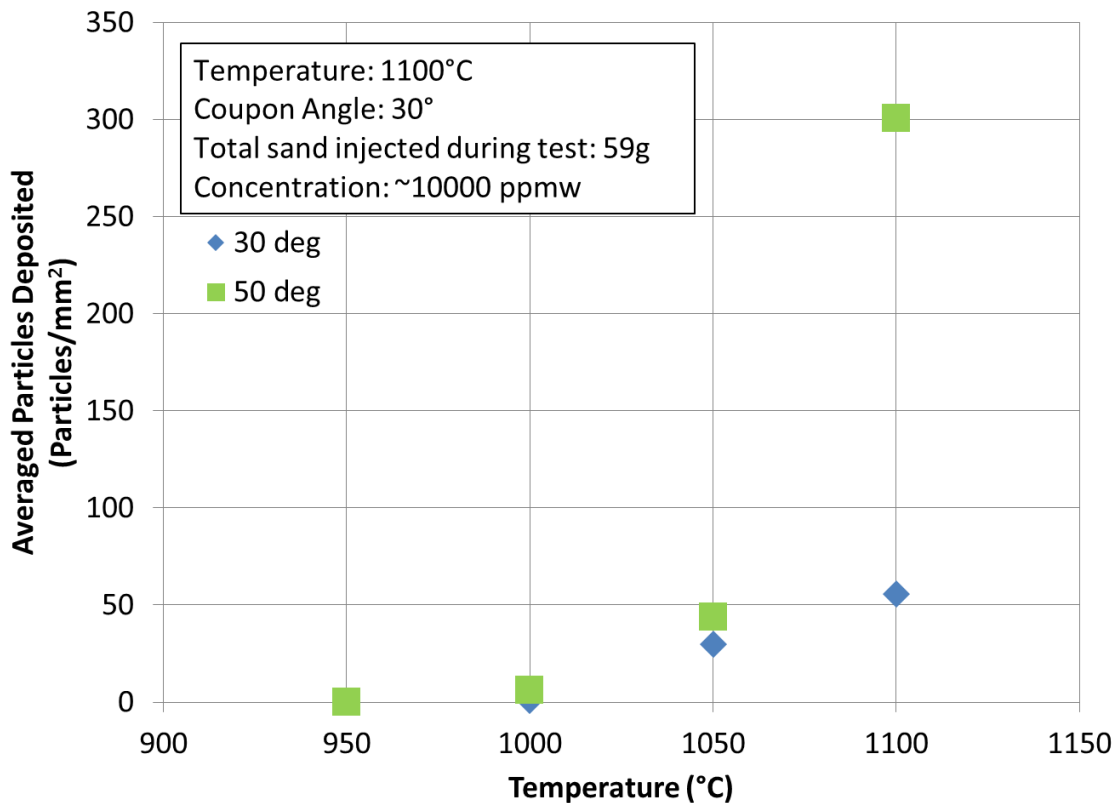


Figure 15. Particle deposition at temperatures ranging from 950°C to 1100°C at 30° coupon angle.

As seen in Figure 14, particle deposition increases drastically with increase in temperature for 50° coupon angle. However, the increase in deposition is not as severe for the 30° coupon angle case. This could be due to particles having lower normal velocity at lower coupon angle. The flow particles could also be affected due to flow field around the test coupon and deviating them tangentially to the coupon surface.

Based on these results, deposition is following the trend observed by Delimont et al. [12] at temperatures up to 1050°C. The deposition is significantly higher at 1100°C compared to 1050°C. This could be due to the impacting particles are above their transition temperature. Moreover, at 50° coupon angle the particles lost significant amount of kinetic energy during impact which could result in majority of particles deforming during impact and sticking to the relatively cooler coupon surface.

4.4 Effect of Impact Angle on Particle Deposition at Constant Temperature

Additional tests were performed using 10g of sand, particle concentration of ~10000 ppmw, 1100°C flow temperature, 70 m/s flow velocity, and coupon angle ranging from 30° to 90°. Results are shown in Figure 16.

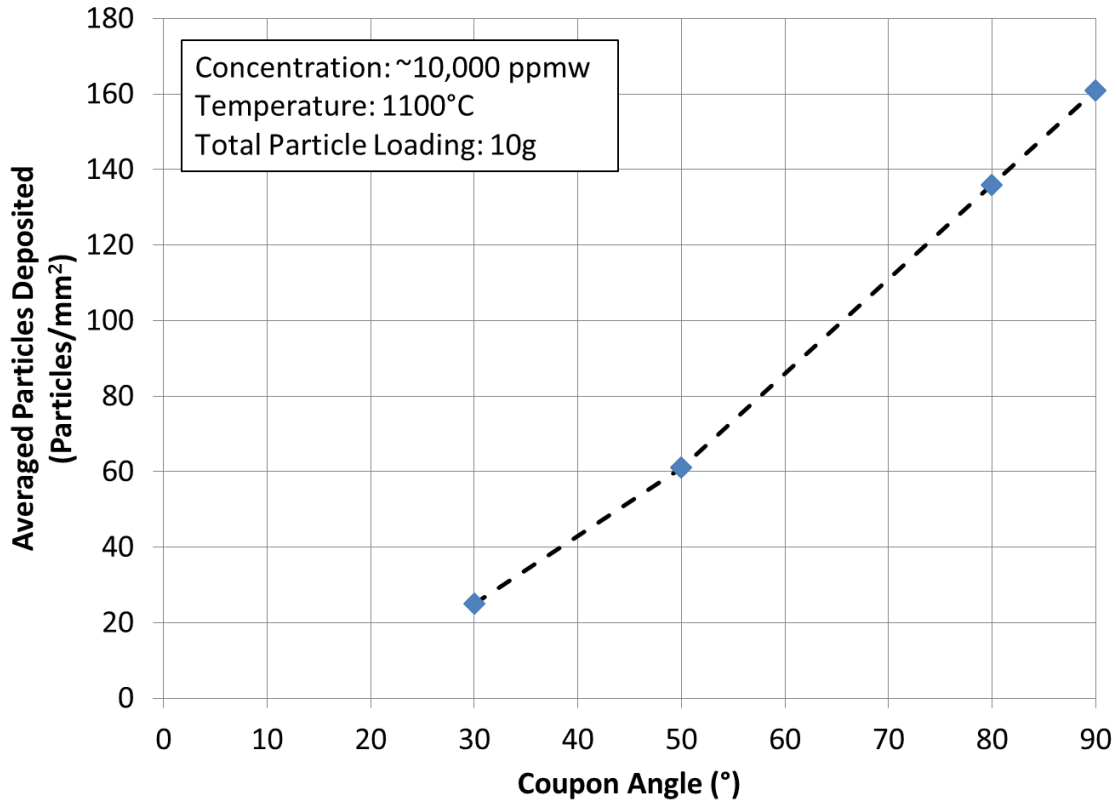


Figure 16. Particle deposition with respect to coupon angle at 1100°C temperature and 10g total sand injected.

As expected, particle deposition increases as the coupon angle increases. However, the increase in deposition is not as severe as seen with 59g sand in previous tests. This could be due to less particles interacting on the coupon surface resulting in less deposition. Based on trends observed by Delimont *et. al.* [12] for change in deposition with respect to coupon angle, the increase in deposition is not as severe with 10g total sand injected. The data is insufficient to explain the reason behind this however, based on the trends observed in Figure 12, the deposition could be drastically different higher amounts of sand is injected during the test.

5. Conclusion

Particle deposition in gas turbine engines is a complex process that depends on the type of particles, temperature, velocity, coupon angle, concentration, total sand injected, etc. This study tests some of these parameters to understand particle deposition at representative engine temperatures. Amount of sand, particle concentration, coupon angle, and temperatures were varied to understand their effects on deposition. It was found that temperature has the most significant impact on particle deposition. Previous studies were performed at near-melting temperatures of the particles and observed a steady increase in deposition at a particular temperature. However, increasing the temperature from 1050°C to 1100°C increased the particle deposition almost six times for the same coupon angle. This is because the particles transition to molten state at temperatures above 1050°C. The overall trend observed in particle deposition was exponential for every 50°C increase in the flow temperature. This study was performed around the temperature at which particles transition to the molten state. It is believed that particle deposition will be drastically higher at higher temperatures. Moreover, it was found that particle concentration used during the study has a direct effect on deposition. The particle deposition almost doubled as the concentration was increased about six times at 30° coupon angle. The deposition could increase more severely at higher coupon angles based on the trend observed in total sand injected and coupon angle analysis performed in this study. This means that accelerated tests to study deposition could be potentially skewed and not replicate actual deposition in turbines accurately. The current study also found that total sand injected has a significant effect on deposition. The deposition is fairly linear up to a total sand injected of 30g. However, increasing total amount of sand to 59g increases the deposition about three times. This increase in deposition for different amounts of sand injected could be significantly different for different coupon angles based on Figure 16. The deposition increased significantly at constant temperature, velocity, concentration, and total sand injected from lower to higher coupon angles. This means that deposition trends observed for different amounts of sand injected and concentration could differ significantly depending on the coupon angle.

More research needs to be done in order to fully understand the effects of total sand injected, concentration, and coupon angle on deposition. The current study shows that deposition increases as these parameters are changed. However, in order to accurately measure the increase

in deposition, effects of total sand injected and concentration need to be measured at different coupon angles and at higher temperatures. Moreover, current experiments were only performed on Hastelloy X bare metal coupon. Rate at which particle deposit is expected to change as the loss in kinetic energy of particles during impact is different on different metals. Moreover, analyzing the deposited particles chemically using SEM or similar techniques may provide insight into the types of compounds that contribute to deposition.

References

- [1] Cowherd, C., 2007, "Sandblaster 2 Support of See-Through Technologies for Particulate Brownout Task 5 Final Technical Report," (110565).
- [2] Jensen, J. W., Squire, S. W., Bons, J. P., and Fletcher, T. H., 2005, "Simulated Land-Based Turbine Deposits Generated in an Accelerated Deposition Facility," *J. Turbomach.*, **127**(3), p. 462.
- [3] Dunn, M. G., 2012, "Operation of Gas Turbine Engines in an Environment Contaminated With Volcanic Ash," *J. Turbomach.*, **134**(5), p. 051001.
- [4] Kim, J., Dunn, M. G., Baran, a. J., Wade, D. P., and Tremba, E. L., 1993, "Deposition of Volcanic Materials in the Hot Sections of Two Gas Turbine Engines," *J. Eng. Gas Turbines Power*, **115**(3), p. 641.
- [5] Bons, J. P., Wammack, J. E., Crosby, J., Fletcher, D., and Fletcher, T. H., 2008, "Evolution of Surface Deposits on a High-Pressure Turbine Blade—Part I: Convective Heat Transfer," *J. Turbomach.*, **130**(2), p. 021021.
- [6] Hamed, a., Tabakoff, W. C., and Wenglarz, R. V., 2006, "Erosion and Deposition in Turbomachinery," *J. Propuls. Power*, **22**(2), pp. 350–360.
- [7] Sieverding, C. H., Tabakoff, W., and Wenglarz, R. A., 1988, *Particulate Flows and Blade Erosion*, von Karmen Institute.
- [8] Licht, W., and Friedlander, S. K., 1977, "Smoke, dust, and haze fundamentals of aerosol behavior," *AIChE J.*, **23**(5), pp. 773–773.
- [9] Smeltzer, C. E., Gulden, M. E., McElmury, S. S., and Compton, W. A., "Mechanisms of Sand and Dust Erosions in Gas Turbine Engines," (August 1970), p. 293.
- [10] Walsh, W. S., Thole, K. a., and Joe, C., 2006, "Effects of Sand Ingestion on the Blockage of Film-Cooling Holes," *Vol. 3 Heat Transf. Parts A B*, **2006**, pp. 81–90.
- [11] Reagle, C. J., Delimont, J. M., Ng, W. F., and Ekkad, S. V., 2013, "Study of Microparticle Rebound Characteristics Under High Temperature Conditions," *J. Eng. Gas Turbines Power*, **136**(1), pp. 011501–011501.
- [12] Delimont, J. M., Ng, W. F., Ekkad, S. V, Tafti, D. K., Lowe, T., and Pickrell, G. R., 2014, "Experimental Investigation of Temperature Effects on Microparticle Sand Rebound Characteristics at Gas Turbine Representative Conditions," p. 186.
- [13] Borom, M. P., Johnson, C. a., and Peluso, L. a., 1996, "Role of environmental deposits and operating surface temperature in spallation of air plasma sprayed thermal barrier coatings," *Surf. Coatings Technol.*, **86-87**(PART 1), pp. 116–126.

- [14] Smialek, J. L., Archer, F. a., and Garlick, R. G., 1992, "The Chemistry of Saudi Arabian Sand - A Deposition Problem on Helicopter Turbine Airfoils."
- [15] Crosby, J. M., Lewis, S., Bons, J. P., Ai, W., and Fletcher, T. H., 2008, "Effects of Temperature and Particle Size on Deposition in Land Based Turbines," *J. Eng. Gas Turbines Power*, **130**(5), p. 051503.
- [16] Borom, M. P., Johnson, C. A., and Peluso, L. A., 1996, "Role of Environmental Deposits In Spallation of TBC on Aeroengine and Land-Based Gas Turbine Hardware."
- [17] Maier, I., Pressures, H., Cole, S., Dioxide, C. T., Rase, D. E., and Roy, R., 1975, "Phase Equilibria in the System," **88**(1932), pp. 34–37.
- [18] Delimont, J. M., Murdock, M. K., Ng, W. F., and Ekkad, S. V., 2014, "GT2014-25687 Effect of Temperature on Microparticle Rebound Characteristics at Constant Impact Velocity," pp. 1–11.
- [19] Bons, J. P., Wammack, J. E., Crosby, J., Fletcher, D., and Fletcher, T. H., 2008, "Evolution of Surface Deposits on a High-Pressure Turbine Blade—Part II: Convective Heat Transfer," *J. Turbomach.*, **130**(2), p. 021021.
- [20] Nealy, D. a., Mihelc, M. S., Hylton, L. D., and Gladden, H. J., 1983, "Measurements of heat transfer distribution over the surfaces of highly loaded turbine nozzle guide vanes," **106**(January 1984), pp. 149–158.
- [21] Cochran, W. G., 1977, "Sampling Technologies," Book, (Third Edition), p. 342.
- [22] Bartlett, J. E., Kotrlik, J. W. K. J. W., and Higgins, C., 2001, "Organizational research: Determining appropriate sample size in survey research appropriate sample size in survey research," *Inf. Technol. Learn. Perform. J.*, **19**(1), p. 43.
- [23] Licht, W., and Friedlander, S. K., 1977, "Smoke, dust, and haze fundamentals of aerosol behavior," *AIChE J.*, **23**(5), pp. 773–773.

A. Appendix: APPL Building Modifications

VT Aerothermal Rig was previously housed at VT Montgomery Airport Lab in the Red Brick Building. The rig was moved from red brick building to APPL in August 2014. The advantage of the APPL building was that it was new and the test cell was built keeping test rig's need in mind. The disadvantage was that the building was still in its final phases of completion and all the support systems such as compressed air, cooling water system, exhaust duct, cooling tower, pump connections, etc. had to be designed and installed. This required significant coordination with VT Corporate Research Center as only their contractors can legally make any modifications to the building.

First, the Kaeser CS 75 Compressor and Buffer Tank were moved from the VT Airport Lab and installed at APPL. The compressor can supply maximum flow rate of 0.3 lbm/s at 120 psi. This compressor was repurposed to be used for shop air at APPL. Since the main compressors were not operational at that time, a temporary line was installed to provide compressed air to the test rig. This was done using 1 inch hose connected directly to the buffer tank via compression fitting. The 1 inch hose would supply compressed air to the secondary buffer tank inside the test cell. Another major critical modification to the compressor was building a shed around it. The Kaeser compressor is meant to operate indoors and can get severely damaged due to wind, snow, and freezing temperatures. The shed is also temporary and protects the compressor from elements. Figures 17 show the compressor, buffer tank, and the 1 in hose connection.



Figure 17. Kaeser CS 75 compressor repurposed to supply shop air at APPL. The shed protects the compressor from rain and snow.

Cooling System

A water cooling system is one of the most critical systems for Aerothermal Rig operation. The burner has an outer jacket through which cooling water flows to keep the walls at a reasonable temperature during operation. The water also cools flow turbulator inside the burner and prevents its inside walls from overheating or melting. Since APPL was in its final stages of completion, there was no cooling system setup for the building. Doing that is a long and costly process that would require co-ordination with CRC and contractors. Hence in order to get the rig operational temporarily, a cooling system was designed and installed at APPL that would provide water to the rig using the same pump and cooling tower used in the Airport lab. About 350 feet of piping and hoses were specified and purchased. The pump supplying water is powered by a 5 hp motor and supplies water 180 gpm with 90 ft head. It was very critical to ensure that water has enough head to go through the burner and the cooling tower after going through 350 ft of piping. The pump is also designed to operate indoors and had to be operated in the open at APPL. A wooden shipping container was repurposed to house the pump and protect it from rain and snow temporarily. The

cooling tower dissipates heat from returning water and also acts as a reservoir. Water is supplied to the pump from the cooling tower and the cooling tower is equipped with a water supply line that supplies water at 5 gpm at low pressure. The cooling tower automatically recharges with a ball-valve mechanism if the water goes below specified level. Figure 18 below show the cooling system at APPL.

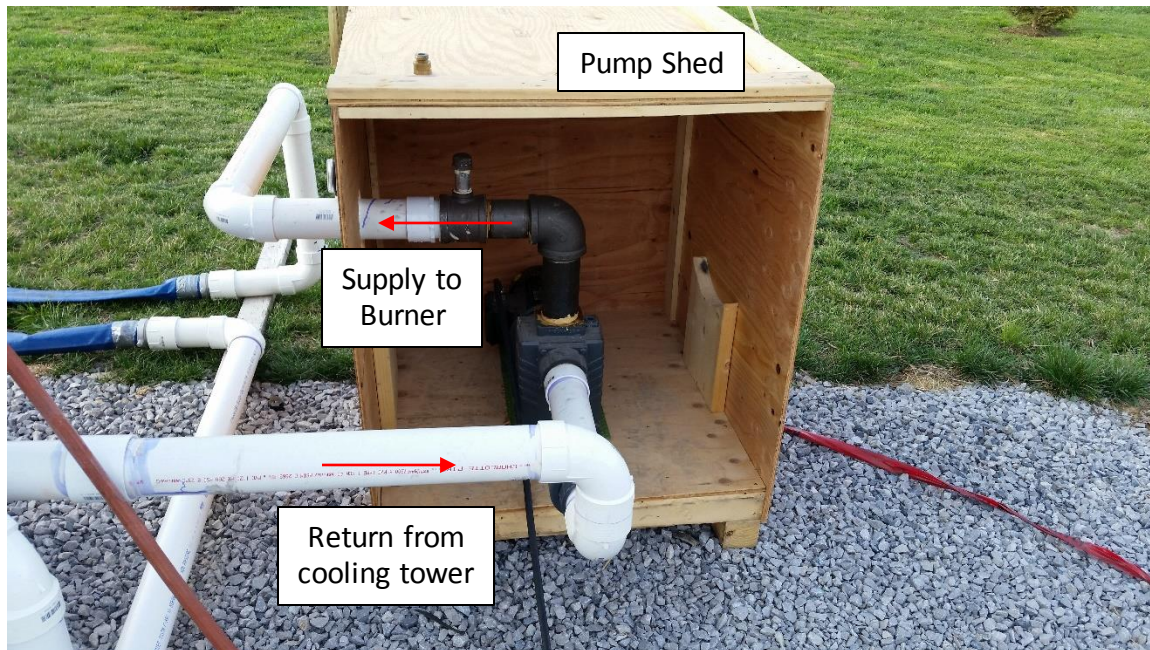


Figure 18. The pump for supplying cooling water housed in a repurposed shipping container. The container protects the pump from rain and snow.

B. Appendix: Aerothermal Test Rig Modifications

The test rig was originally purchased in August 1967 by Allison Division of General Motors Company and the last results from Rolls-Royce, Indianapolis were published in 1988. The rig was received by Virginia Tech in September 2010 and has been repurposed to perform coefficient of restitution and deposition measurements [11]. In August of 2014, the test rig was moved to APPL from its original location at VT Airport. At APPL, the test rig was setup to be able to operate at same capacity as the previous location. Significant changes have been made to the test rig and APPL and are documented in this section.

The test section part of the test rig expands noticeably when operating at very high temperatures based on previous experience. This expansion exerts additional stresses on the test section support and the exhaust duct. These stresses could severely damage test section support and the wall on which the exhaust duct is supported. At Indianapolis, the gooseneck on the test section would act as an expansion joint and was constrained to a concrete wall specially made for this purpose. However, this was not possible at APPL. Moreover, exhaust hole at APPL was off-centered by about 13 inches with respect to the exhaust duct on the test rig. Fixing this would require changes to decades old test section or raising the height of the test rig. Installing a rail system for the test rig would not only raise its height but also provide a mechanism to allow the test section roll back and forth during thermal expansion. Hence a 24' long V-channel rail was designed, manufactured, and installed at APPL. The rail worked extremely well when moving heavy test rig components. The rails are made from extra thick 4" I-beams that has a factor of safety of ~5. Special rail carts were also designed and manufactures to hold the burner and the test section of the Aerothermal rig. Figure 19 below shows an image of rail in the test cell. Carts allowed to adjust the burner and the test section in lateral direction as it is very critical to align them in a straight line to allow proper installation of the equilibration tube.

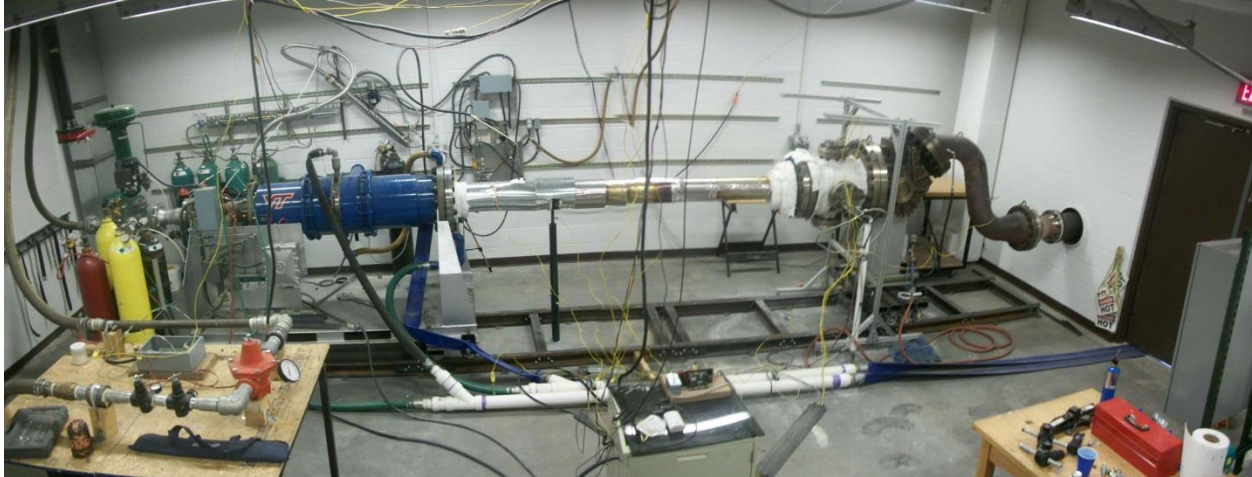


Figure 19. The Aerothermal rig on rails at APPL.

i. LabVIEW Safety Loops

The Aerothermal test rig is controlled using a LabVIEW code and has physical and logical safety locks in it. These safety locks have been incorporated in the hardware and LabVIEW code over the years' based on experiences. The test rig is monitored using thermocouples and pressure transducer that send signal voltages to NI CompactDAQ. Readings from these instruments are used to monitor the rig. A small loophole in the rig operation was uncovered during one of the tests. There was nothing to prevent accidentally opening the fuel valve fully. This will allow huge amounts of methane in the test rig and can lead to catastrophic combustion of methane throughout the test rig. Moreover, it was also discovered that there was no safety lock to ensure that the air was flowing through the test rig before starting the pilot flame or injecting methane. Flowing air through the rig is critical before any type of combustion as it mitigates pressure shocks generated during ignition and prevents the rig hardware from getting damage. In order to fix this, two safety loops were added to the LabVIEW code that would 1) Prevent any sort of fuel supply and ignition in the test rig if the main valve was closed and 2) The main valve cannot be closed if there is combustion going in the test rig.

Moreover, additional thermocouples and CCTV cameras were installed to measure burner operation and monitor rig inside the test cell when it is being operated. Figure 20 below shows the screenshot of the updated LabVIEW code.

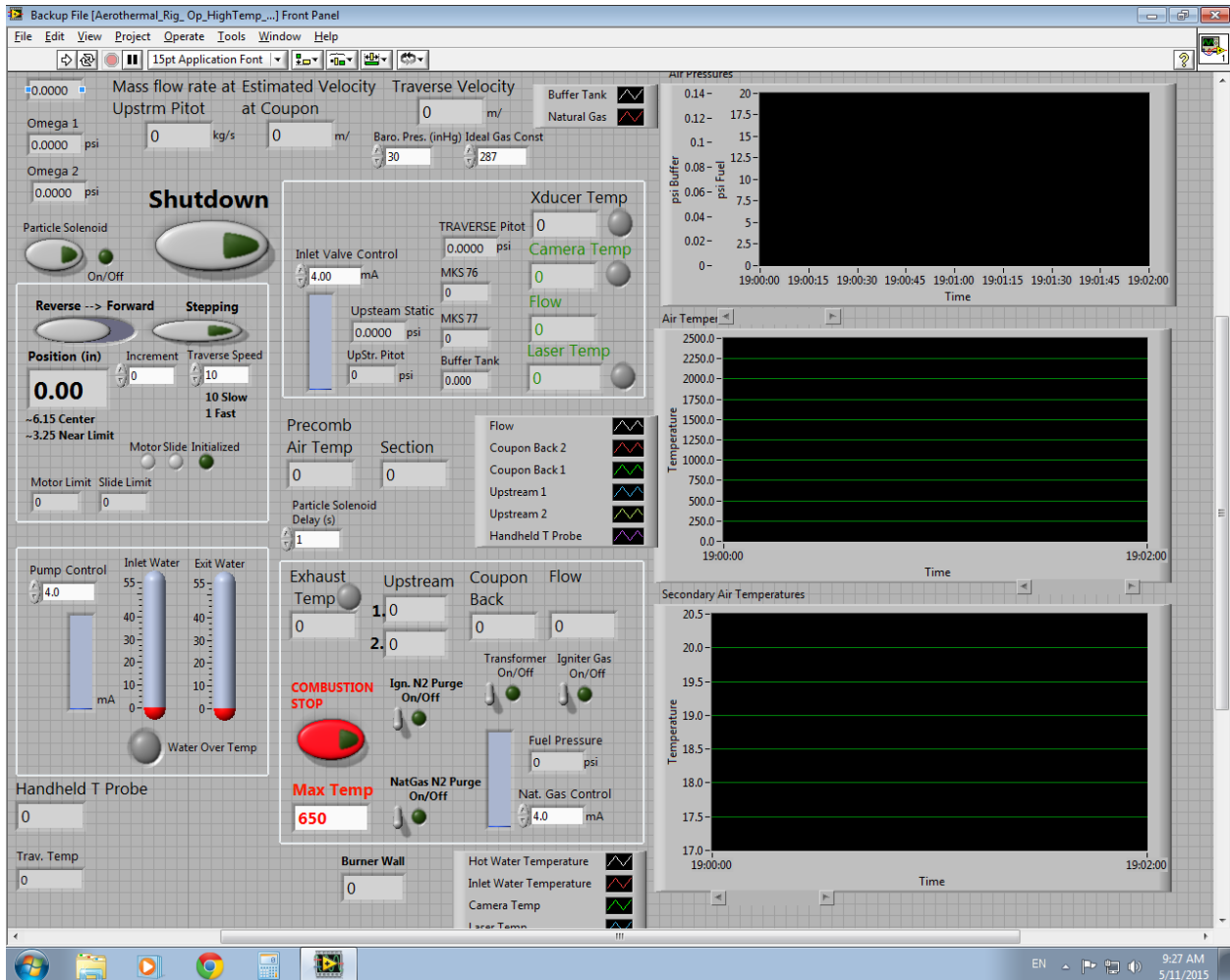


Figure 20. Screenshot of LabVIEW VI with suggested changes. Additional thermocouples were mounted on the burner wall for monitoring purposes.

ii. Fuel and Particle Delivery System

A special wooden wall structure was built at the VT Airport lab to mount the pipes, valves, regulators, and hoses for particle injector system. Same support was later used to mount the fuel lines and fuel valves as well. These systems are necessary for safe operation of the rig and new support structure was needed to be built at APPL to mount the particle and fuel delivery systems. Since these systems were already made and working, the support had to match the mounting locations of the existing system so it can be re-used. To solve this problem, strut channels were mounted along the length of a test-cell wall adjacent to the test rig. The strut channels gave the flexibility to have mounting location at any point on the wall and were able to support the weight

of the equipment as well. Figure 21 shows the fuel and particle delivery systems mounted to the strut channels inside the test cell.

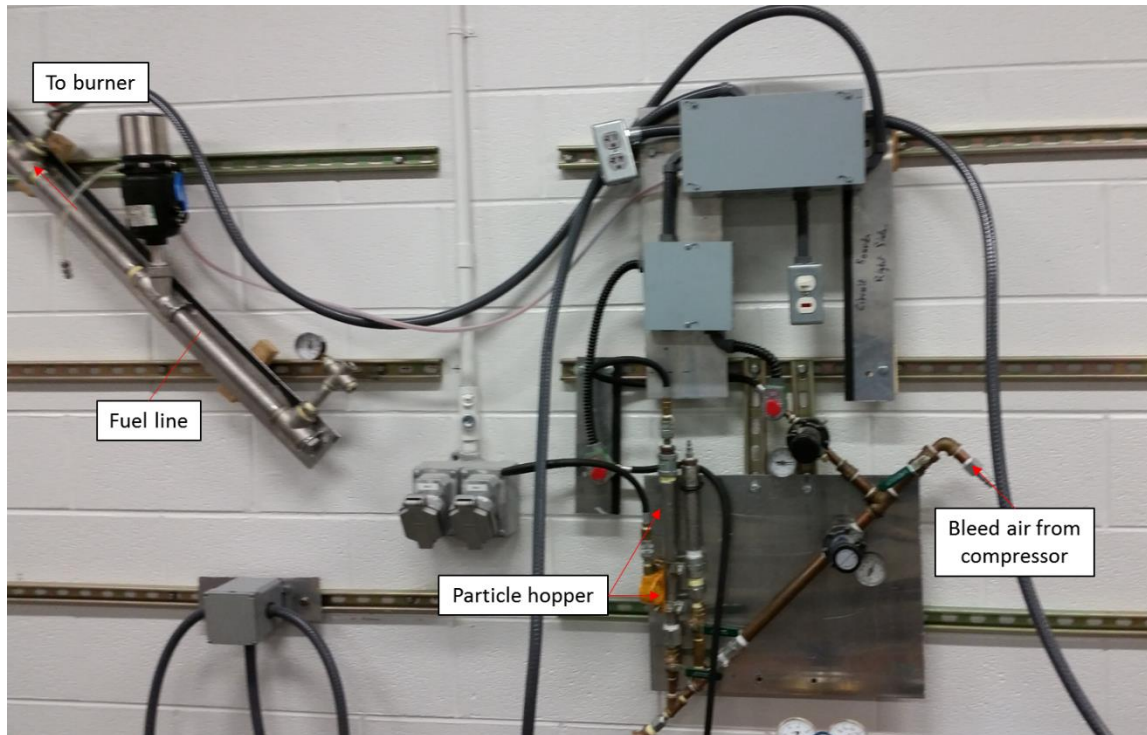


Figure 21. The fuel supply to the Aerothermal Rig is remotely controlled using the pneumatic valve and the particles are injected in to the rig through the particle hopper.

C. Appendix: MATLAB Particle Counter Code

The MATLAB code to count individual particles in an image was developed by Dr. Jacob Delimont and Matt Murdock [8, 9] and all credit goes to them. The code transforms the original colored image to black and white and then inverts it. In the inverted image, the particles appear to be bright spots that the code can recognize. The user specifies a range for the size of the particles in pixels. The code looks for bright spots of that size and finds counts them. Since the particles are not perfectly spherical, the code is not able to count all the particles sometimes. In this case, the user has the option to select the left out particles towards the end and then the code will include these particles to its initial counting.

```
%% Determine Number of particles
clear all
close all
%Read image
[file, rootname] = uigetfile('*.bmp','Select the test image... ');
a=imread([rootname file]);
b=a;

% scrsz = get(0,'ScreenSize');
% figure('Position', scrsz);
% imagesc(a); set(gca, 'DataAspectRatio', [1 1 1])
% title('Find Masking Edge')
% colormap(flipud('gray'));
% set(gca,'YDir','reverse')
% strf{1} = 'Please select visible edges of coupon...';
% strf{2} = '...Then press enter (*Delete removes last selection)';
% t = text(40, 100, strf, 'BackgroundColor', [1 1 1]);
% parts = impixel; %selects coupon points on edge
% delete(t); clear WhoCares1;

SIZE=size(a);
psize = 200;
minsize = 100;
light1 = 0;
%Convert to grayscale
a=rgb2gray(a);

figure;
imshow(a);
index = size(a);

i=1;
j=1;
light=mean(mean(a))
for i=1:index(1)
    for j=1:index(2)
```

```

        if a(i,j) > light/2 || a(i,j) <1
            a(i,j) = 256;
        end
    end
end

figure;
imshow(a);
%Threshold the image
a2=im2bw(a,graythresh(a));
%Other Filtera
% a1 = medfilt2(a,[2 2]);
% figure()
% imshow(a1)
%
% a1 = wiener2(a1,[5 5]);
% figure(2)
% imshow(a1)
%
% a1 = imadjust(a1,[],[],.1);
% figure(4)
% imshow(a1)

% a1 = bpass(a,0,psize);
% figure(5)
% imshow(a1)

%Negative
a1=~a2;
%Filter
a1 = medfilt2(a1,[30 30]);
% figure
% imshow(a1)
%%
pk1 = pkfnd(a1,light1,psize);
afill=zeros(SIZE(1)+2*psize,SIZE(2)+2*psize);
index=size(afill);
i=1;
j=1;
for i=1:index(1)-1
    for j=1:index(2)-1
        if i>psize && i<index(1)-psize && j>psize && j<index(2)-psize
            afill(i,j) = a1(i-psize,j-psize);
        end
    end
end
end
% figure
% imshow(afill)
pk2=pk1+psize;
cnt1 = cntrd(afill,pk2,psize+4);
[I,m]=size(cnt1);
j=1;
for i=1:I
    if cnt1(i,4)>= (minsize/2.5)^2 && cnt1(i,3) >=400;
        pos1(j,:)=cnt1(i,:);
        j=j+1;
    end
end

```

```

    end
end

figure
imshow(afill);
axis on
hold all
% axis([0 SIZE(1) 0 SIZE(2)]);
xlabel('Pixels'); ylabel('Pixels');
% plot(pos1(:,1),pos1(:,2),'or','MarkerFaceColor','r')
% plot(cnt1(:,1),cnt1(:,2),'og')
% plot(pk2(:,1),pk2(:,2),'ob')
hold off
number_particles = size(pos1,1)

figure
imshow(b);
axis on
hold all
% axis([0 SIZE(1) 0 SIZE(2)]);
xlabel('Pixels'); ylabel('Pixels');
plot(pos1(:,1)-psize,pos1(:,2)-psize,'ob','MarkerFaceColor','r')
parts = impixel; %selects coupon points on edge
hold off

number_particles = size(pos1,1)+size(parts,1)

% % Find and Draw Boundaries
% B = bwboundaries(a1);
% imshow(a1)
% text(10,10, strcat('\color{red}Objects Found:', num2str(length(B))))
% hold on
%
% for k = 1:length(B)
% boundary = B{k};
% plot(boundary(:,2), boundary(:,1), 'g', 'LineWidth', 0.2)
% end
%
% size(B);

```